Imaging voltage-dependent cell motions with heterodyne Mach–Zehnder phase microscopy

Christopher Fang-Yen,[1,*] Seungeun Oh,[1] Yongkeun Park,[1] Wonshik Choi,[1] Sen Song,[2] H. Sebastian Seung,[2] Ramachandra R. Dasari,[1] and Michael S. Feld[1]

[1]*G. R. Harrison Spectroscopy Laboratory, Massachusetts Institute of Technology, Cambridge, Massachusetts 02139, USA*

[2]*Howard Hughes Medical Institute and Department of Brain and Cognitive Sciences, Massachusetts Institute of Technology, Cambridge, Massachusetts 02139, USA*

[*]*Corresponding author: minwah@mit.edu*

Received February 8, 2007; accepted March 26, 2007;
posted April 3, 2007 (Doc. ID 79902); published May 18, 2007

We describe a heterodyne Mach–Zehnder interferometric microscope capable of quantitative phase imaging of biological samples with subnanometer sensitivity and frame rates up to 10 kHz. We use the microscope to image cultured neurons and measure nanometer-scale voltage-dependent motions in cells expressing the membrane motor protein prestin. © 2007 Optical Society of America

OCIS codes: 120.3180, 170.3880.

Most biological cells are nearly transparent to light at optical wavelengths and can be imaged in their natural states only via the phase shifts they induce in transmitted light. Microscopy techniques such as phase contrast [1] and differential interference contrast [2] render unstained cells visible by converting these phase shifts into variations in light intensity.

Recently, a number of interferometric and noninterferometric techniques have been developed for *quantitative* measurement of the optical path delays associated with living cells [3–5]. Applications have included mapping the "dry mass" distribution of cells [3], measuring motility and fluctuations in cells [4], measuring cell volume changes [6], and measurement of the cell refractive index [5–7]. Relatively little work has been done on imaging motions of excitable cells, although nonimaging interferometric schemes have been used to measure motions in neurons and myocytes [8–10].

Methods for calculating the phase image include variable spatial filtering [11–13], variable defocusing [14,15], or stepped phase shifting of a reference beam [3,16,17]. Spatial filtering schemes typically place restrictions on illumination geometry and may limit certain spatial frequencies of the phase image. Defocusing and phase-shifting techniques are typically limited in speed. In this paper we describe a quantitative interferometric microscope in which the phase is calculated from a time-dependent interference pattern induced by acousto-optic shifting of a reference beam. This time-domain approach has the advantage of being largely independent of illumination geometry and does not affect spatial resolution.

The setup (Fig. 1) consists of a Mach–Zender laser interferometer integrated with an inverted microscope. A helium–neon laser (Melles Griot) is collimated and divided into sample and reference paths by a beam splitter. The sample beam passes through a microscope consisting of a sample, a 60× objective lens (Olympus SAPO, focal length $f_1 = 3.0$ mm), and a tube lens (focal length $f_2 = 200$ mm). To preserve the phase of the field transmitted through the sample, the distance between the objective and tube lens is set equal to the sum of their focal lengths.

The reference beam passes through two acousto-optic modulators, AOM1 and AOM2, driven at frequencies $\omega_1 = 110.0$ MHz and $\omega_2 = 110.0$ MHz $+ \Omega$, respectively, with Ω variable over $0-10,000$ Hz using a custom-built digitally synthesized RF driver. Irises select the +1- and −1-order diffracted beams, respectively, such that the total reference beam frequency shift is Ω. After passing through the AOMs, the reference beam is spatially filtered and enlarged by a beam expander.

A beam splitter recombines the sample and reference fields, which are incident on a complementary metal-oxide semiconductor camera (Photron 1024PCI). The irradiance at the image plane consists of a "rolling" fringe pattern due to interference between the magnified sample field and the frequency-shifted reference plane wave:

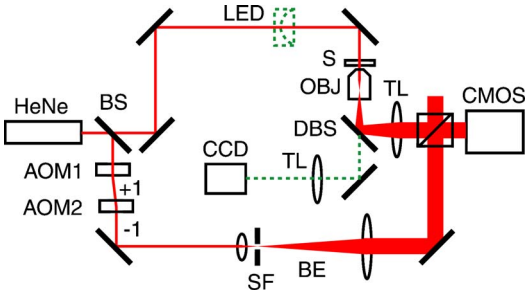

Fig. 1. (Color online) Heterodyne Mach–Zehnder phase microscope. HeNe, helium–neon laser; solid line, laser beam; dashed line, bright-field illumination beam. In the sample path: S, sample; OBJ, objective lens ($f = f_1$); DBS, dichroic beam splitter; TL, tube lenses ($f = f_2$); LED, light-emitting diode bright-field illuminator (removed during interferometry measurements); CCD, camera for bright-field and fluorescence imaging. In the reference path: AOM1,2, acousto-optic modulators; BE, beam expander; SF, spatial filter; CMOS, camera for interferometric imaging. Not shown: mercury lamp fluorescence illuminator and filter cube in the bright-field illumination path.

0146-9592/07/111572-3/$15.00

$$I(x,y,t) = I_S(x,y) + I_R(x,y) + 2\sqrt{I_S(x,y)I_R(x,y)}\cos[\phi_S(x,y,t) + \Omega t],$$

where $I_S(x,y)$, $I_R(x,y)$ are the irradiances of the sample and reference fields, respectively, and $\phi_S(x,y,t)$ is the time-dependent sample phase. The focus and tilt of the sample and reference beams are adjusted to minimize the difference between the two wavefronts. Irradiances at the detector plane were $\sim 10\ \mu W/cm^2$ for both the sample and reference fields. Exposure times were typically $\sim 50\ \mu s$.

Demodulation of the time-dependent phase signal was performed by one of two methods: (i) In the Hilbert transform technique, a complex representation of the sample phase is calculated via $z_S(x,y,t) = (I(x,y,t) + iH[I(x,y,t)])\exp(i\Omega t)$ where H is the Hilbert transform, $I(x,y,t)$ represents the time-dependent raw image data, and the exponential term compensates for the heterodyne signal. (ii) In the phase-shifting interferometry technique, the frame rate is set to exactly four times the heterodyne frequency, such that consecutive frames differ in phase by $\pi/2$. For each sequence of four consecutive images I_1, I_2, I_3, and I_4, a complex representation of the sample phase can be calculated via $\phi_S(x,y,t) = \arg z_S(x,y,t)$, with $z_S(x,y,t) = (I_4 - I_2) + i(I_3 - I_1)$. The two methods gave identical results except for slightly different noise characteristics, which will be described elsewhere.

To reduce the effects of temporal phase noise between the sample and reference paths, the sample phase is measured relative to a reference region R in the field of view. We let $z_R(t) = \int_R z_S(x,y,t)dxdy$ and calculate the relative sample field via $\phi_S(x,y,t) = \arg(z_S(x,y,t)/z_R(t))$. A background phase image from an area devoid of the sample was subtracted to reduce spatial phase nonuniformity. Two-dimensional phase unwrapping was performed using Goldstein's algorithm [18].

To demonstrate the instrument's capabilities for cell imaging, we obtained quantitative phase images of a rat hippocampal neuron, cultured as previously described [19]. The phase-shifting interferometry demodulation technique was used. The cell body and nerve fibers are clearly resolved (Fig. 2).

As part of our investigation of voltage-dependent cell motions, including motions in neurons [8], we used the heterodyne interferometer to image voltage-dependent motions in cells expressing the motor protein prestin. Prestin, the motor protein of the cochlear outer hair cells [20], directly transduces changes in the transmembrane voltage to membrane motions [21]. Previous measurements of electromotility in transfected cells have used a photodiode occlusion technique [20] or atomic force microscopy [22]. Since these methods assay motion only at single points, it was not possible to image the spatial distribution of electromotility or determine the spatial modes of oscillation.

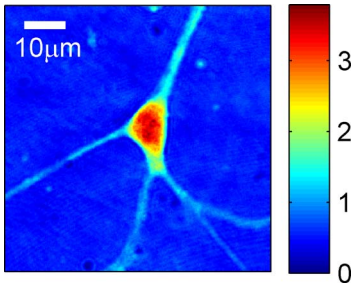

Fig. 2. (Color online) Phase image of a cultured rat hippocampal neuron. Phase in radians.

In our experiments, human embryonic kidney (HEK 293) cells were transfected with a plasmid coding for a fusion between gerbil prestin and green fluorescent protein (GFP) using Effectene transfection reagent (Qiagen). Electromotility experiments were performed 3–7 days after transfection. Cells were detached from culture dishes using Cellstripper (Mediatech), suspended in phosphate buffered saline (PBS), and drawn by suction into fire-polished, PBS-filled glass micropipettes with a 5–6 μm tip diameter.

Sinusoidal electrical stimulation with frequency 200–250 Hz and amplitude 400–600 mV (peak-to-peak) was delivered to the cell through the micropipette using a patch clamp amplifier (Multiclamp 700A, Axon Instruments) for a duration of 1.7 s. Time-dependent phase image data for a 96×96 pixel ($24.5\ \mu m \times 24.5\ \mu m$) field of view were collected using the Hilbert transform technique with frame rate 6000 frames/s and heterodyne frequency 600 Hz. Figure 3(a) shows a phase image of a cell in a microchamber stimulated at 217 Hz frequency and 400 mV (peak-to-peak) amplitude. Some phase unwrapping errors appear due to the large index contrast and thickness of the micropipette but do not affect our time-dependent phase measurements.

To probe for electromotility signals, we binned the phase data into 5×5 pixel ($1.275 \times 1.275\ \mu m$) regions of interest (ROIs). Figure 3(c) shows the power spectrum of the phase at three such ROIs: (1) at the edge of the cell, (2) at the glass pipette, and (3) at a point separated from both cell and pipette. Each is measured with the fourth ROI used as the reference region R. The phase from region (1) displays a sharp peak at the stimulation frequency, indicating voltage-dependent motions. The microchamber holding the cell shows no peak at this frequency, ruling out artifacts from pipette motion. Baseline noise levels are typically 0.2 mrad/$Hz^{1/2}$, corresponding to displacements of approximately 20 pm/$Hz^{1/2}$.

To analyze the spatial dependence of electromotility, we calculated the in-phase amplitude at the stimulus frequency for every ROI in or near the cell, with the in-phase defined relative to the phase of the maximum signal. Typical data are shown in Fig. 3(b). Signal amplitudes are largest near the upper and lower boundaries of the cell, and two sides are seen to be moving in opposite phase laterally in the pipette. Comparison of the frequency-dependent phase signals with the spatial gradient of phase images from the same cells leads to an estimate of electromotility amplitude of 10 nm for the cell shown in Fig. 3. Electromotility signals were observed in roughly 60% of

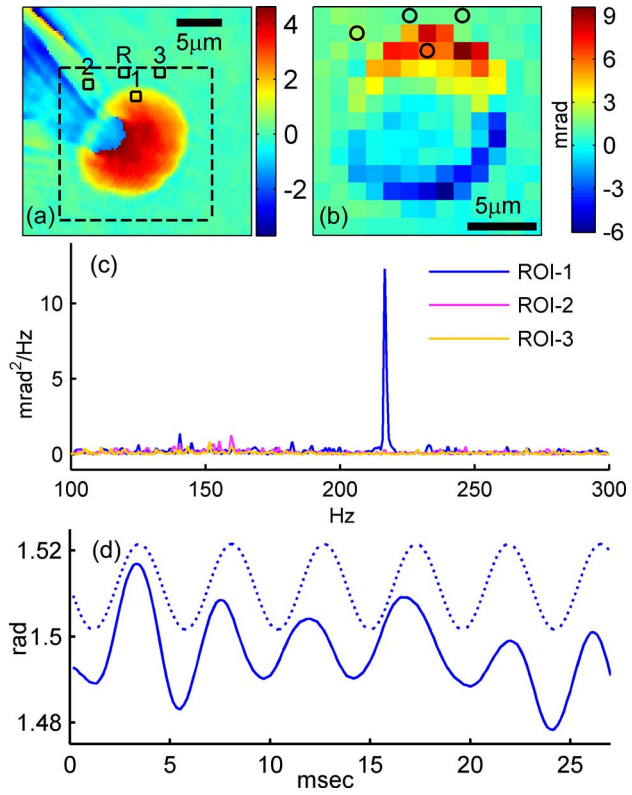

Fig. 3. (Color online) (a) Phase image of prestin-transfected HEK 293 cell in a micropipette. Squares, regions of interest (ROI) labeled 1–3 and reference region R. Phase in radians. (b) Map of the in-phase component of fast Fourier transform at stimulus frequency 217 Hz. ROIs are denoted by circles. (c). Power spectra of the phase signals from ROIs 1–3. (d) Solid line, time trace of phase of ROI-1 referenced by ROI-R; dashed line, 217 Hz, 20 mrad peak-to-peak amplitude sine wave.

transfected cells tested and varied in peak amplitude from 1 to 5 mrad. For all cells showing responses, the spatial dependence of electromotility signals was similar to that shown in Fig. 3. Nontransfected control cells displayed no measurable electromotility.

The measurement of transverse cell motions is in contrast with other studies of prestin-induced electromotility, in which longitudinal motions along the axis of the stimulation pipette were assumed [20,22]. Lateral motion may result from asymmetries in the distribution of prestin, adherence of the cell membrane to the microchamber, or the mechanical properties of the cell. These imaging results suggest that single-point measurements alone may not accurately describe the amplitudes of voltage-dependent oscillations.

In summary, we have developed a time-domain imaging interferometer with high sensitivity and bandwidth and used it to perform imaging measurements of electromotility in prestin-transfected cells. Current and future work includes a detailed study of cellular electromotility and its correlation with nonlinear capacitance, an electrical property of prestin-transfected cells that is often taken to represent electromotility, and measurement of voltage-dependent motions in neurons and other excitable cells.

The authors thank Peter Dallos (Northwestern University) for providing the plasmid for prestin–GFP and Carlos Lois for assistance with cell culture procedures. This work was supported by the National Institutes of Health (P41-RR02594-18) and Hamamatsu Corporation.

References

1. F. Zernike, Physica **9**, 686 (1942).
2. G. Nomarski, J. Phys. Radium **16**, 9S (1955).
3. G. A. Dunn and D. Zicha, J. Cell. Sci. **108**, 1239 (1995).
4. G. Popescu, T. Ikeda, C. A. Best, K. Badizadegan, R. R. Dasari, and M. S. Feld, J. Biomed. Opt. **10**, (2005).
5. N. Lue, G. Popescu, T. Ikeda, R. R. Dasari, K. Badizadegan, and M. S. Feld, Opt. Lett. **31**, 2759 (2006).
6. B. Rappaz, P. Marquet, E. Cuche, Y. Emery, C. Depeursinge, and P. J. Magistretti, Opt. Express **13**, 9361 (2005).
7. B. Kemper, D. Carl, J. Schnekenburger, I. Bredebusch, M. Schafer, W. Domschke, and G. von Bally, J. Biomed. Opt. **11**, 34005 (2006).
8. C. Fang-Yen, M. C. Chu, H. S. Seung, R. R. Dasari, and M. S. Feld, Opt. Lett. **29**, 2028 (2004).
9. T. Akkin, D. P. Dave, T. E. Milner, and H. G. Rylander, Opt. Express **12**, 2377 (2004).
10. M. A. Choma, A. K. Ellerbee, C. H. Yang, T. L. Creazzo, and J. A. Izatt, Opt. Lett. **30**, 1162 (2005).
11. T. Ikeda, G. Popescu, R. R. Dasari, and M. S. Feld, Opt. Lett. **30**, 1165 (2005).
12. G. Popescu, T. Ikeda, R. R. Dasari, and M. S. Feld, Opt. Lett. **31**, 775 (2006).
13. G. Popescu, L. P. Deflores, J. C. Vaughan, K. Badizadegan, H. Iwai, R. R. Dasari, and M. S. Feld, Opt. Lett. **29**, 2503 (2004).
14. E. D. Barone-Nugent, A. Barty, and K. A. Nugent, J. Microsc. **206**, 194 (2002).
15. A. Barty, K. A. Nugent, D. Paganin, and A. Roberts, Opt. Lett. **23**, 817 (1998).
16. X. H. Li, T. Yamauchi, H. Iwai, Y. Yamashita, H. J. Zhang, and T. Hiruma, Opt. Lett. **31**, 1830 (2006).
17. H. Iwai, C. Fang-Yen, G. Popescu, A. Wax, K. Badizadegan, R. R. Dasari, and M. S. Feld, Opt. Lett. **29**, 2399 (2004).
18. R. M. Goldstein, H. A. Zebker, and C. L. Werner, Radio Sci. **23**, 713 (1988).
19. A. Starovoytov, J. Choi, and H. S. Seung, J. Neurophysiol. **93**, 1090 (2005).
20. J. Zheng, W. Shen, D. Z. He, K. B. Long, L. D. Madison, and P. Dallos, Nature **405**, 149 (2000).
21. P. Dallos and B. Fakler, Nat. Rev. Mol. Cell Biol. **3**, 104 (2002).
22. J. Ludwig, D. Oliver, G. Frank, N. Klocker, A. W. Gummer, and B. Fakler, Proc. Natl. Acad. Sci. U.S.A. **98**, 4178 (2001).